Structure and Dynamics of the Full-Length Lipid-Modified H-Ras Protein in a 1,2-Dimyristoylglycero-3-phosphocholine Bilayer

5 AUTHORS, INCLUDING:

Alemayehu A Gorfe
University of Texas Medical School at Houston

75 PUBLICATIONS **1,660** CITATIONS

SEE PROFILE

Michael Hanzal-Bayer
University of Queensland

15 PUBLICATIONS **1,010** CITATIONS

SEE PROFILE

Daniel Abankwa
Åbo Akademi University

42 PUBLICATIONS **1,272** CITATIONS

SEE PROFILE

Structure and Dynamics of the Full-Length Lipid-Modified H-Ras Protein in a 1,2-Dimyristoylglycero-3-phosphocholine Bilayer

Alemayehu A. Gorfe,*[†,‡] Michael Hanzal-Bayer,[⊥] Daniel Abankwa,[⊥] John F. Hancock,[⊥] and J. Andrew McCammon[†,‡,§,‖]

Department of Chemistry and Biochemistry, Center for Theoretical Biological Physics, Howard Hughes Medical Institute, and Department of Pharmacology, University of California at San Diego, La Jolla, California 92093-0365, and Institute for Molecular Bioscience, University of Queensland, Queensland 4072, Australia

Ras proteins regulate signal transduction processes that control cell growth and proliferation. Their disregulation is a common cause of human tumors. Atomic level structural and dynamical information in a membrane environment is crucial for understanding signaling specificity among Ras isoforms and for the design of selective anti-cancer agents. Here, the structure of the full-length H-Ras protein in complex with a 1,2-dimyristoylglycero-3-phosphocholine (DMPC) bilayer obtained from modeling and all-atom explicit solvent molecular dynamics simulations, as well as experimental validation of the main results, are presented. We find that, in addition to the lipid anchor, H-Ras membrane binding involves direct interaction of residues in the catalytic domain with DMPC phosphates. Two modes of binding (possibly modulated by GTP/GDP exchange) differing in the orientation and bilayer contact of the soluble domain as well as in the participation of the flexible linker in membrane binding are proposed. These results are supported by our initial in vivo experiments. The overall structures of the protein and the bilayer remain similar to those of the isolated components, with few localized structural and dynamical changes. The implications of the results to membrane lateral segregation and other aspects of Ras signaling are discussed.

Introduction

Ras proteins are GTPases that operate as binary switches in signal transduction pathways. They control such crucial cellular functions as proliferation and differentiation by cycling between a guanine diphosphate (GDP)-bound "off" state and guanine triphosphate (GTP)-bound "on" state. Upon activation by growth factors, guanine nucleotide exchange factors (GEF)[a] interact with GDP-bound Ras, catalyzing the release of GDP and rapid binding of the more abundant GTP. GTP loading induces a conformational change in Ras,[1,2] triggering interactions with a variety of down-stream effectors. Binding of the negative regulators called GTPase activating proteins (GAP) to the GTP-bound Ras terminates the signal flow by accelerating the slow intrinsic hydrolysis of GTP. A molecular defect in Ras impairs the ability of the Ras−GAP complex to hydrolyze GTP, leading to uncontrolled cell growth or cancer.

H-Ras is a small (189 amino acids) protein, which, together with N- and K-Ras, belongs to the Ras subfamily of the p21 Ras superfamily. It is active only when bound to membranes (mainly at the inner surface of plasma membranes). Membrane binding is achieved through three post-translational lipid modifications. H-Ras undergoes farnesylation at Cys186 in the CAAX box (where A represents aliphatic and X any amino acid)

followed by proteolysis of the AAX tripeptide and carboxymethylation at the C-terminal farnesylated cystein. A subsequent reversible palmitoylation at Cys181 and Cys184 produces the lipid-anchor[3] for tight membrane binding (Figure 1a). The roles of the catalytic soluble domain (residues 1−166, G-domain), the linker (residues 167−179), and the lipid-anchor (residues 180−186) in membrane targeting and affinity have been biochemically characterized.[4] It was observed that the lipid-anchor and the linker generate high-affinity attractive forces for lipid raft and non-raft domains, respectively.[4] The effect of the G-domain on the lateral segregation of H-Ras on plasma membranes was found to be modulated by GDP/GTP exchange; the GDP-bound form preferentially localizes at lipid rafts, while the GTP-bound form segregates to disordered regions.[5] The activated G12V variant of H-Ras populates non-raft domains. Furthermore, a recent hypothesis suggests that Ras proteins induce organization of actively regulated dynamic nanoclusters rather than binding into pre-existing microdomains on the inner surface of plasma membranes.[6]

The structure of the soluble part comprising the N-terminal 166 or 171 residues of H-Ras has been solved in both the GTP (or analogues)- and the GDP-bound forms for the wild-type[7−11] and a number of oncogenic mutants[12−14] (similarly for its complexes with GAPs[15] and GEFs[16,17]). Recently, Thapar et al. explored the effect of the linker sequence and farnesylation on the soluble domain of an H-Ras variant that has three Cys-to-Ser substitutions.[18] This solution NMR study lacks the possible effects of a membrane environment and palmitoyl modifications. Nonetheless, it showed that the extreme C-terminal region perturbs the structure of the soluble domain.[18] Some progress is also being made in understanding the Ras−membrane interaction. For example, based on studies of short peptides containing the C-terminal membrane-binding segments of N-Ras, detailed structural and dynamical information on the membrane-binding mechanism of Ras proteins is emerging.[19−21] However, neither the structure of the full-length membrane-

---

* To whom correspondence should be addressed. Phone: (858) 822-0255. Fax: (858) 534-4974. E-mail: abebe@mccammon.ucsd.edu.
† Department of Chemistry and Biochemistry, University of California at San Diego.
‡ Center for Theoretical Biological Physics, University of California at San Diego.
§ Howard Hughes Medical Institute, University of California at San Diego.
‖ Department of Pharmacology, University of California at San Diego.
⊥ University of Queensland.
a Abbreviations: DMPC, 1,2-dimyristoylglycero-3-phosphocholine; GAP, guanine nucleotide activating protein; GEF, guanine nucleotide exchange factor; HVR, hypervariable region; MD, molecular dynamics; NMR, nuclear magnetic resonance; rmsd, root-mean-square deviation; RMSF, root-mean-square fluctuation.
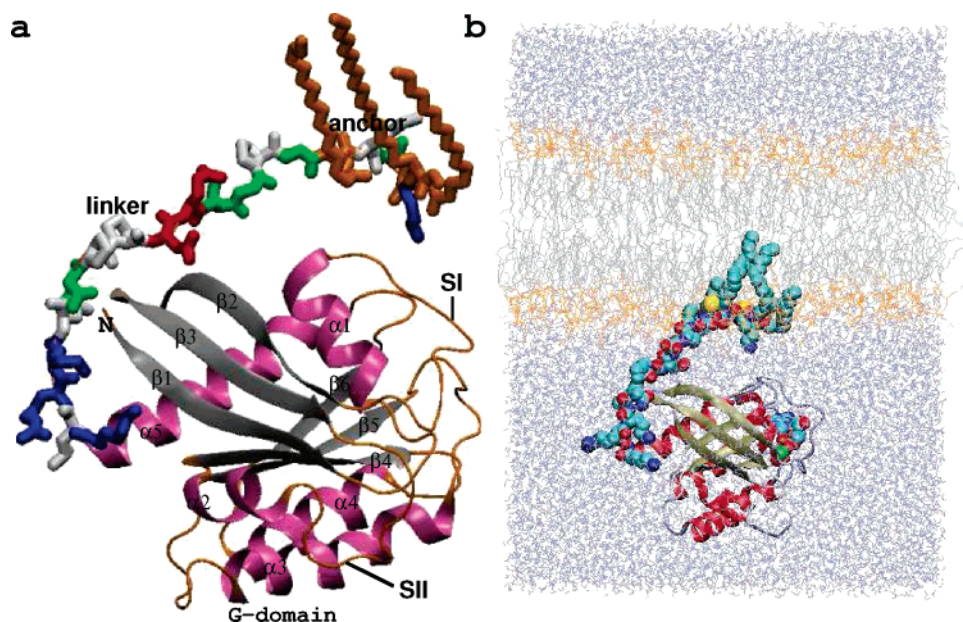
Figure 1. (a) A model of the full-length H-Ras protein. The G-domain is in a cartoon representation, and the modeled C-terminal residues are in stick models colored in red (acidic), blue (basic), green (polar), gray (apolar), and orange (lipid modified residues). The secondary structure elements and the switch loops SI (residues 25−40) and SII (residues 60−70) are labeled. (b) System setup. The solvated and equilibrated H-Ras−membrane complex with the DMPC head groups and lipid tails in yellow and silver, respectively. The protein is in a cartoon representation except for the C-terminal 21 residues and the $Mg^{2+} \cdot GDP$ cofactor, which are in atom-colored space filling model. The water is in light blue.

bound H-Ras protein nor an atomic level description of the interactions governing the affinity of each Ras structural segment for the plasma membrane is available. Similarly, very little is known about the structure and dynamics of the membrane in the presence of bound Ras. NMR and crystallographic approaches to address these issues faced significant challenges due to C-terminal proteolysis and thiol oxidation of the protein.[18] On the other hand, computations have provided substantial insights into a number of protein−membrane complexes (e.g., refs 22, 23).

Based on results from modeling and all-atom explicit solvent molecular dynamics (MD) simulations, this report proposes a complete picture of the full-length H-Ras protein in complex with a 1,2-dimyristoylglycero-3-phosphocholine (DMPC) bilayer. The relative orientations of the catalytic domain and the flexible linker with respect to the membrane are investigated. Novel mechanisms of membrane binding that involve, in addition to the lipid anchor, direct interaction of residues in the G-domain or the linker with phosphate head groups are presented. The two dominant modes of protein−membrane interactions differ in protein orientation, in the extent of interaction with the phosphate head groups, and in the degree of active participation of the flexible linker. The relative population of the two modes appears to be modulated by GTP/GDP exchange. Complex formation did not significantly affect the global structure, relative to the isolated components, of the protein and the bilayer. However, we found localized structural and dynamical changes in the protein and the DMPC. Validation of some of the main computational results by our initial experiments and the implications for Ras signaling and lateral segregation are discussed.

Results and Discussion

The main focus of this paper is the structural characterization of the membrane-inserted full-length H-Ras protein based on results from modeling and simulations. To monitor self-consistency and to avoid potential artifacts (e.g., of force field origin), we ran control simulations for the pure DMPC bilayer

**Table 1.** DMPC Bilayer Structural Properties[a]

sim. name	dmpc	hvr	fl.gdp	fl.gtp	experiment[ref]
$D_{PP}(z)$ [Å]	36.4 ± 0.2	36.5 ± 0.2	36.2 ± 0.2	36.2 ± 0.2	$36.0,^{50}\ 35.2^{51}$
$L_{C2:C2}(z)$ [Å]	25.3 ± 0.2	25.5 ± 0.2	25.2 ± 0.2	25.2 ± 0.2	$25.2,^{50}\ 25.4^{51}$
$L_{C2:C14}(z)$ [Å]	11.3 ± 0.1	11.3 ± 0.1	11.3 ± 0.1	11.5 ± 0.1	11.0^{19}

a Data are obtained by averaging over snapshots of 10 ps interval excluding the first 15 ns. Two slightly different experimental values for the bilayer thickness and hydrophobic thickness are shown: (i) fully hydrated fluid phase DMPC (2zPC and 2DC in Table 2 of Kucerka et al.;[51] the corresponding area/lipid was 60.6 Å), and (ii) L_α DMPC bilayer (DHH and 2DC in Table 6 of Tristram-Nagle and Nagle;[50] corresponding area/lipid estimate was 59.6 Å). The chain length is compared to that estimated by Huster et al.[19] on the basis of a slightly lower (due to peptide insertion) average order parameter of 0.167 Å; hence the actual chain length may be slightly higher. All of the experimental data are at 30 °C.

and for the soluble, catalytic domain (G-domain, residues 1−166) in water. An insertion simulation of only the hypervariable region (HVR, residues 167−186) is performed to compare its structure and membrane-binding properties in the absence and presence of the G-domain. We use the available biochemical data[4,5,24] and the NMR study of the farnesylated full-length H-Ras by Thapar et al.[18] together with the current in vivo experiments, to validate the simulation results.

Overview of the Simulations. Membrane Structure. The ensemble averaged structural properties of the membrane (see Methods), such as the average bilayer thickness ($D_{PP}(z)$), the hydrophobic thickness ($L_{C2:C2}(z)$), and the chain length ($L_{C2:C14}(z)$), are in excellent agreement with experimental measurements (Table 1). Their time evolution (not shown) also indicated that the bilayer structure is well stabilized. The deuterium order parameters (S_{CD}) are also in very good agreement with experiments and previous simulations (Figure 2a). Overall, the simulated membrane structures properly model the liquid crystalline (L_α) phase of a DMPC bilayer, and the insertion simulations behaved similar to the neat DMPC simulation.

Protein Structure. Figure 2b plots the time evolution of the C_α root-mean-squared deviations (rmsd) of the G-domain (residues 1−166) with respect to the starting X-ray structure. As compared to simulations in water, it took longer for the rmsd
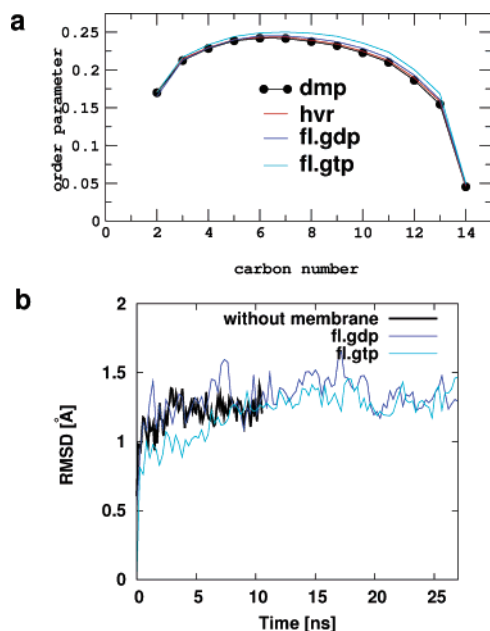
Figure 2. Structural properties of the membrane and of the protein. (a) Calculated order parameters (see eq 1). (b) Time evolution of the root-mean-squared deviation (rmsd) from the starting structure. Only C_α atoms of the residues at the G-domain (1−166, excluding switches I and II) are included.

to equilibrate in the membrane-bound simulations (∼3 ns versus > 15 ns). However, the small deviations in all cases suggest that the protein catalytic domain maintains its overall structure during membrane insertion.

Predicting the Structure of the Hypervariable Region. The hypervariable C-terminal region (HVR) comprises the linker and membrane binding regions. Despite its role in function and in the compartmentalization of membrane-bound H-Ras,[4,25] however, the structure of the membrane-bound HVR is not known. In solution, residues 173−185 were shown to be conformationally averaged.[18] Membrane binding might reduce the conformational variability. The HVR can thus be expected to have a preferred geometry, likely existing as an ensemble of conformations separated by low-energy barriers. Could the simulations generate such an ensemble? To answer this question, we carried out a detailed structural analysis of the HVR before dealing with the whole complex. For ease of comparison with experiments, the HVR is subdivided into HVR1 (residues 167−172), HVR2 (173−179), and anchor (180−186).[4,25]

First, the C_α rmsds with respect to the equilibrated starting conformations were calculated (Figure 3a). Substantial fluctuations are observed in simulation hvr, whereas in fl.gdp and fl.gtp the rmsd was stabilized after 15 ns at ∼5 and ∼4 Å, respectively. Second, pairwise C_α rmsds for all snapshots after 15 ns (10 ps interval) were calculated for each trajectory, and the resulting distributions are plotted in Figure 3b with the corresponding structures summarized in the inset. It is immediately clear that, after 15 ns, each of the full-length simulations predominantly sampled a small locale of the conformational space and generated ensembles of structures with an average deviation between members of 1−1.5 Å. In contrast, no preferred conformations were achieved in the absence of the G-domain (hvr) within the 30 ns time scale. Third, the snapshots from all of the trajectories (again excluding the first 15 ns) were combined and clustered on the basis of the rmsd (cutoff 2 Å). The two most populated clusters are displayed in Figure 3c.

Taken together, we find that HVR adopts a coil−bend−coil overall structure with highest flexibility and bending occurring
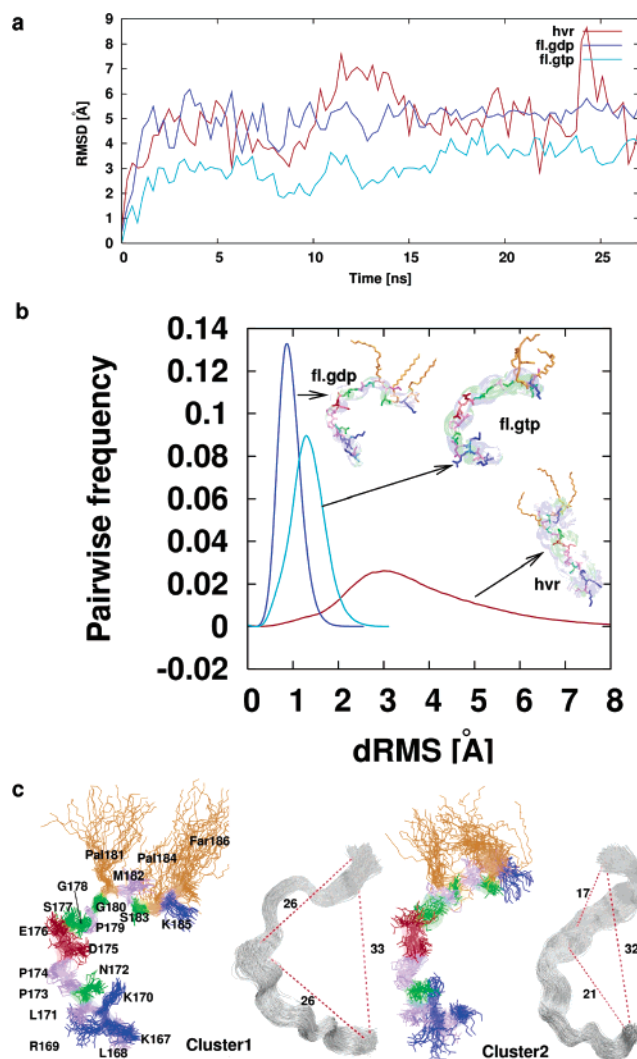
Figure 3. The structure of the hypervariable region (residues 167−186). (a) Time evolution of C_α rmsds measured from the respective equilibrated structures. (b) The distribution of the pairwise (snapshot-by-snapshot, 10 ps interval) C_α rmsd (dRMS). Insets show the superposition of 100 ps-separated snapshots with the last snapshot in sticks. (c) Superposition of structures obtained from C_α rmsd-based clustering of the combined snapshots. The two most populated clusters are shown. Lines (left side) represent side-chain orientations, while the tubes represent the overall shape of the segment. Distances between C_α atoms of the terminal residues (K167 and C186) and the middle of the segment (S177) are labeled. Data from the first 15 ns are excluded in (b) and (c).

at HVR2 within the amino acid stretch of P173−P174−D175−E176−S177. The anchor and HVR1 are less mobile. The most stable conformations look like semicircles with an end-to-end distance of >30 Å. This conformation is stabilized by the G-domain through a strong salt-bridge between side chains of K170 of the linker and D49 of strand β2. Note that, although α5 elongates to R169 in the starting structure[26] and was suggested to extend to residue 172 in solution,[18] its occurrence beyond H166 is sporadic in the simulations. It would be interesting to determine whether this is due to the force field or the inherent flexibility of residues 167−171. On the 173−185 segment, our results in a membrane environment agree with those of solution NMR,[18] but do not support an earlier prediction of a helical hairpin structure.[27] Note also that the anchor side chains adopt specific orientations: K185 and S183 point outward, while M182 and the acyl chains orient into the DMPC core (upward). HVR1 side chains also have preferred orienta-
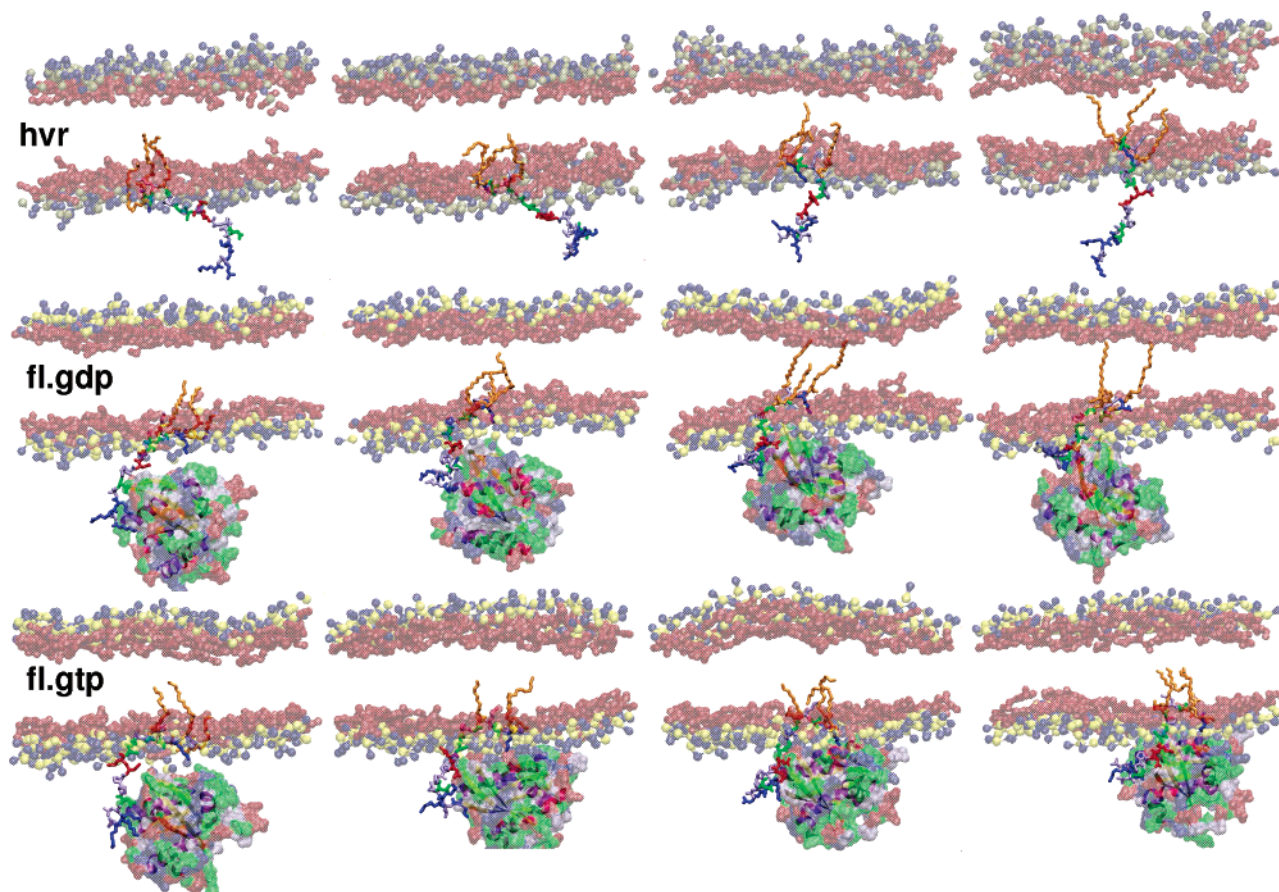
Figure 4. Membrane insertion. (a) Snapshots (at 0.2, 10, 20, and 27 ns) showing the progress of membrane insertion and binding in simulations hvr (top), fl.gdp (middle), and fl.gtp (bottom). Only selected atoms of the DMPC (phosphorus (yellow), nitrogen (blue), and glycerol oxygens (red)) are shown for clarity. The transparent surface and cartoons show the soluble part of the protein, whereas C-terminal HVR residues are shown in stick representation (color code as in Figure 1).

tions, especially in cluster1. We conclude that, in the presence of the catalytic domain, the HVR segment adopts a few clearly defined backbone conformations with specific side-chain orientations.

H-Ras−DMPC Complex. The setup of the simulations (see methods) enabled complete membrane insertion of the protein in nanosecond time scales. The snapshots in Figure 4 provide an overview of the insertion process. Membrane binding by the full-length H-Ras and by only the HVR segment is qualitatively similar, suggesting that membrane insertion of H-Ras is primarily due to the anchor (residues 180−186), and in agreement with experimental data that the anchor segment alone provides sufficient attractive force for a high-affinity plasma-membrane binding.[4] In fact, the total number of protein atoms within 4.0 Å of those of DMPC atoms is similar in the presence and absence of the G-domain (not shown). In all cases, the Ras acyl chains and the hydrophobic M182 side chain insert deep into the hydrophobic core of the DMPC. The polar side chains S183/K185 and the backbone reside close to the DMPC−water interface. However, the simulations differ in the role and arrangement of the linker residues 167−179. Part of the linker, especially HVR1, remains in water in simulation hvr, interacts with the DMPC head groups in fl.gdp, but wraps around the G-domain when GDP is replaced by GTP (i.e., fl.gtp). In the latter, the G-domain directly interacts with DMPC. These results suggest that (i) there are two possible modes of membrane binding by H-Ras, and (ii) the relative population of the two may be modulated by GDP/GTP exchange. Subsequent sections will first provide the details of the membrane localizations of the different protein subdomains and then the atomic interactions

responsible for those localizations followed by experimental evidence for the functional role of some of the interactions.

Membrane Localization. The electron density plots of Figure 5a show that backbone atoms of the anchor reside close to the DMPC glycerol oxygen atoms in all three simulations. However, the peaks (average locations) and the width of the distributions vary. The Gaussian distributions in fl.gdp and fl.gtp indicate an approximately horizontal orientation of the anchor (see Figure 3) with its backbone lying beneath and above the glycerol oxygens, respectively. The wide distribution in hvr reflects the extended structure of the HVR in the absence of the G-domain (Figure 3). Side chains of the linker did not penetrate past the DMPC phosphates in all cases (not shown), whereas those of the anchor (including its lipid tails) have a wide distribution, up to $z = 10.0$ Å in fl.gdp and hvr, and $z = 0.0$ Å in fl.gtp, indicating that the acyl chains populate either nearly the entire hydrophobic core or just the lower leaflet, respectively. The normalized histograms of the methyl (i.e., C16) carbon atom positions shown in Figure 5b indicate how deep the Ras lipid tails penetrate the bilayer.

Several observations can be made from Figure 5. First, both the backbone and the lipids of H-Ras lipid anchor insert deeper into plasma membranes than does the dual lipidated heptapeptide representing the N-Ras lipid anchor,[19,20] or K-Ras (Gorfe and McCammon, unpublished). Second, the membrane-insertion level of the anchor is modulated by the G-domain, whose membrane interaction in turn appears to be modulated by GDP/GTP exchange. This observation is consistent with differential protection of the C-terminus ("switch III") in oncogenic and cellular H-Ras suggested by the slower depalmi-
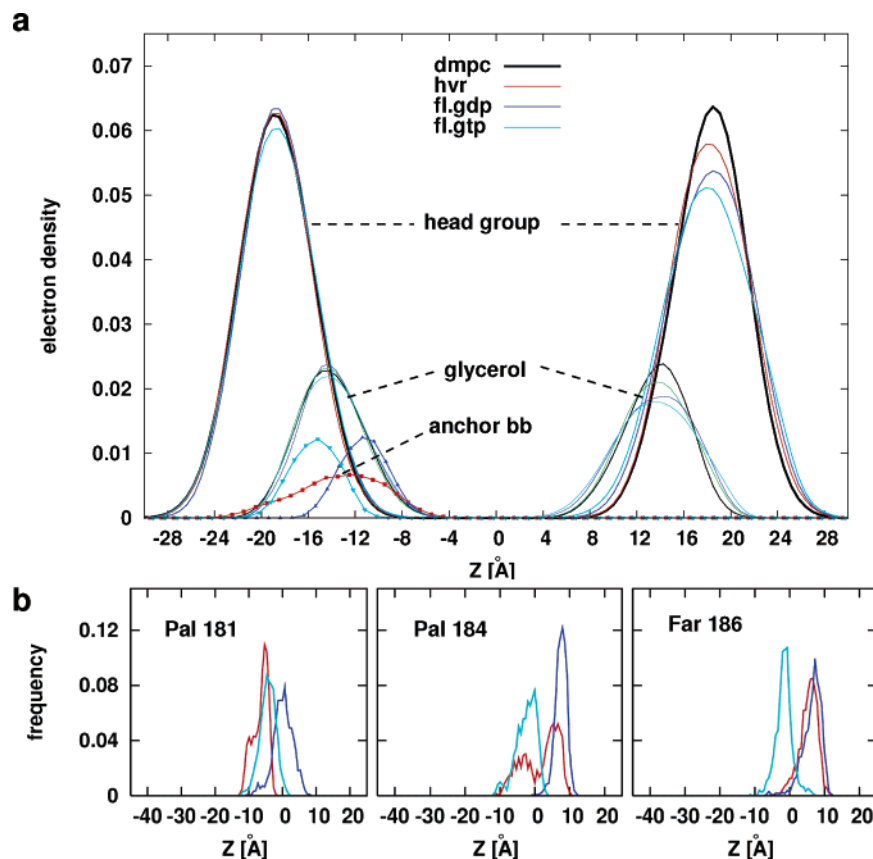
Figure 5. Membrane localization of H-Ras. Electron density plots (a), and normalized histogram of the C16 methyl carbon atom positions (b), along the *z*-axis. Lines represent DMPC head group, glycerol oxygen, and protein side-chain atoms. Symbols designate protein backbone atoms.

toylation rate of the latter.[28] Third, the degree of membrane core penetration by the two palmitoyl groups is not the same. Whether such a variation relates to the experimentally observed differences in the lateral segregation of the Cys181 and Cys184 mono-palmitoylated H-Ras[29] is an interesting question awaiting a deeper investigation.

Protein–Membrane Interactions. What are the atomic interactions that lead to the two modes of membrane binding and the specific localizations of the different protein subunits described above? In a previous work on the heptapeptide from N-Ras membrane anchor, we showed that van der Waals (vdW) interactions between Ras peptide and DMPC lipids, as well as between apolar side chains and DMPC acyl chains, provide the major driving force for binding. The interfacial localization of the backbone enabled hydrogen-bonding interactions with the phosphate head groups.[20] Similarly, vdW interactions involving the three Ras lipids and M182, supplemented by hydrogen-bonding interactions involving the backbone, are responsible for anchoring H-Ras on plasma membrane. Because of the deeper insertion of the anchor, however, H-Ras backbone is hydrogen bonded mainly with the glycerol carbonyls.

As mentioned above, in both fl.gdp and fl.gtp, the major interaction between the G-dromain and the linker involves a salt bridge between E49 (at $\beta 2$) and K170 side chains. However, additional interactions render the relative orientation of the G-domain and the linker with respect to the bilayer totally different. These include a hydrogen bond between the N-terminus and D175 carboxyl in fl.gdp, and G48 carbonyl with the amide of S177 in fl.gtp. The resulting pattern of the linker and the G-domain's interactions with the bilayer surface is completely different, giving rise to two modes of membrane binding (models 1 and 2, Figure 6a and b). In model 1, the protein interacts with the DMPC surface through several residues

at the HVR1 and the N-terminus as well as residues at the $\beta 2$-$\beta 3$ loop of the G-domain. In model 2, the protein makes a larger contact surface involving parts of $\alpha 4$ and $\alpha 5$. Of special interest may be the hydrogen bonds of positively charged residues with the DMPC phosphates. The major ones are R169 and K170 in model 1, and R128 and R135 as well as other polar side chains in helices $\alpha 4$ and $\alpha 5$ in model 2 (Figure 6).

A Functional Role for Residues 128, 135, 169, and 170 Is Confirmed in Vivo. To validate our model further, we analyzed the functional role of residues R169 and K170 (model 1) and R128 and R135 (model 2) in vivo. To this end, we generated alanine substitution mutants for each pair, either alone or in combination, in constitutively active H-RasG12V. The constructs were then transiently transfected into PC12 cells, and Ras-induced cell differentiation was assayed (Figure 7). PC12 cell neurite outgrowth stimulated by RasG12V is a well-established model system to quantify Ras signal output. As shown previously,[25] substitution of amino acids 167–172 with alanines (HVR1Ala, a positive control) inhibited H-Ras signaling and neurite growth. Interestingly, alanine substitution of R128,R135 and R169,K170 residue pairs had opposing effects on H-Ras-mediated neurite outgrowth (Figure 7). Alanine substitution of R128,R135 produced a small decrease in H-ras signal output, comparable to that of the HVR1Ala mutant protein (although with lower statistical significance). In contrast, alanine substitution of R169,K170 caused a large, statistically significant increase in mean neurite length (Figure 7). Importantly, a construct combining all four mutations showed no effect when compared to H-RasG12V, suggesting that these residue pairs have antagonizing effects (Figure 7).

On the basis of our modeling results, we hypothesize that the two protein conformations observed in models 1 and 2 reflect two end states of an equilibrium that, in addition to the known
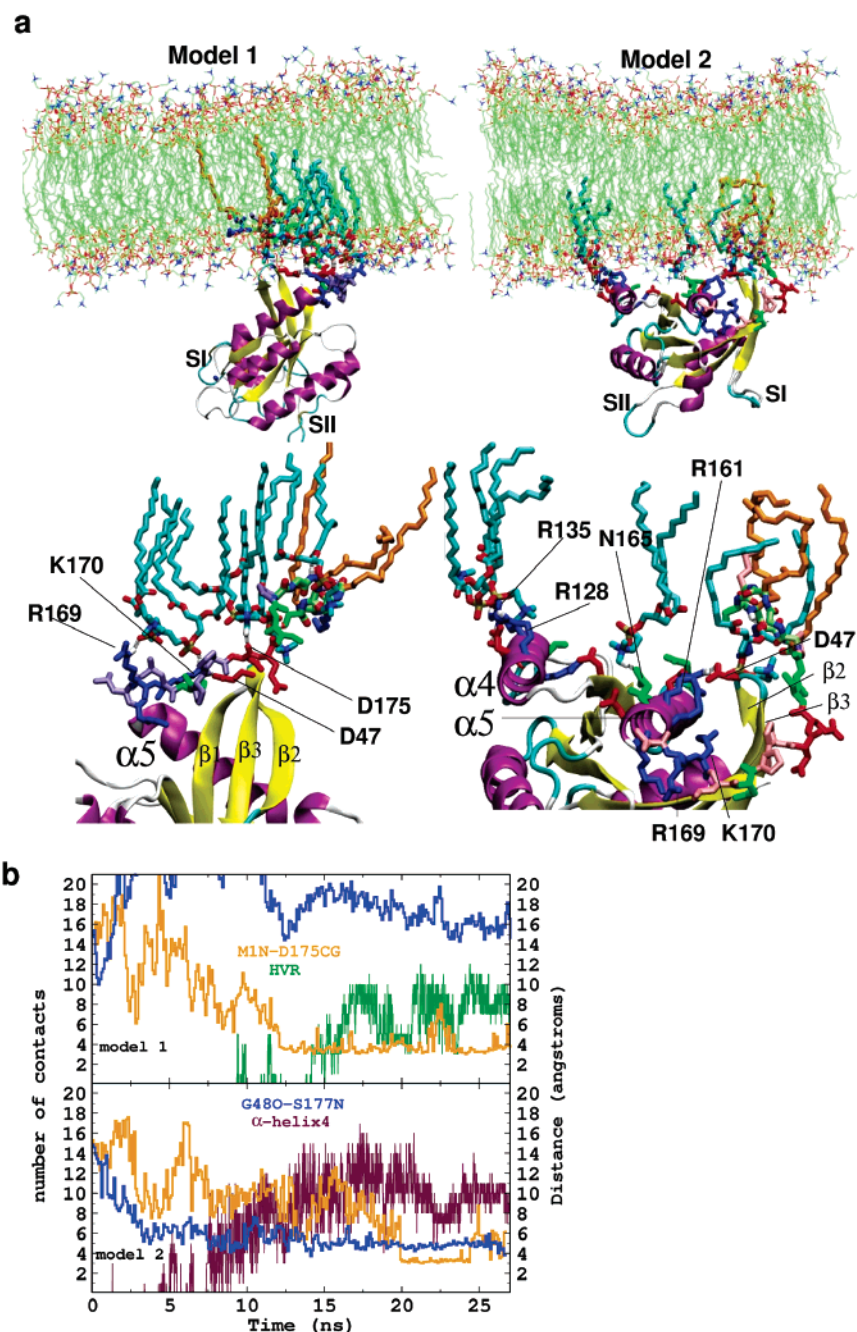
Figure 6. Full-length H-Ras bound to a DMPC bilayer. (a) Two modes of binding, models 1 (left) and 2 (right), are derived from the simulations. The whole protein−bilayer (top) and a blowup of the interaction sites (bottom) are displayed. Residues of the HVR segment and some of the polar/charged amino acids from the G-domain that are close to the bilayer are shown in sticks. Also in sticks are the DMPC lipids hydrogen bonded to the protein (cyan) and the Ras lipids (orange). The rest of the protein is shown in a cartoon representation and the rest of the lipid in lines with carbon atoms in green, phosphorus in yellow, and oxygen in red. Water molecules and hydrogen atoms are omitted. (b) Left axis, total number of R/K side chain heavy atoms within 4.0 Å of DMPC heavy atoms (number of contacts): shown in green is from R169 and K170 at the hypervariable region (HVR), and in maroon from R128 and R135 at helix α 4. Right axis, distances between selected protein atoms: in blue is between G48 carbonyl and S177 amide, and in gold is between M1 amide and D175 γ-carbon.

conformational changes due to nucleotide exchange, is finely balanced by antagonizing contacts between the membrane and the residues newly identified in this study. As H-RasG12V is locked in the GTP-bound conformation in our PC12 assays, it may more accurately be described by model 2. Contacts between the membrane and residues R169 and K170 potentially destabilize this conformation and shift the equilibrium toward model 1, whereas their removal could potentially further stabilize model 2. These effects would account for the enhanced signaling capability of H-RasG12V with alanine substitutions at R169 and K170. Residues R128 and R135, on the other hand, may

further stabilize the "signaling competent" model 2 conformation but with lower affinities. Consistent with the larger contact surface observed in model 2 (Figure 6), additional polar side chains in helices α4 and α5 may be important. Clearly, additional experimental clarification is needed, but our initial studies strongly support a previously unknown, functional role of residues 128, 135, 169, and 170.

Localized Structural Perturbations. The overall structure of the G-domain is stable and the equilibrium structural properties of the bilayer are similar in the simulations with and without inserted protein (Figure 2a,b and Table 1). Now we
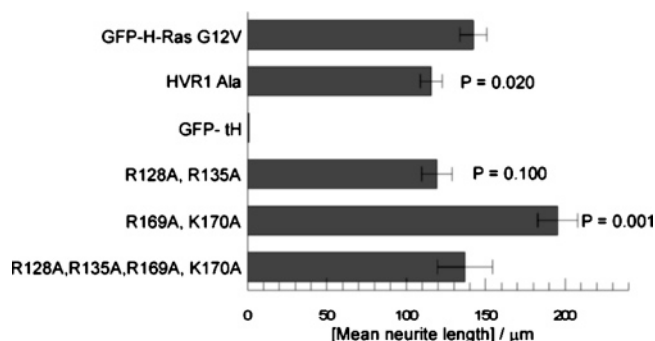
Figure 7. Biological activity of HVR and α 4-point mutations. The biological activity of H-rasG12V with and without 128,135A and 169,170A mutations was determined in a PC12 cell differentiation assay. The graph shows mean neurite length of 52 cells (±s.e.m) transiently expressing the indicated constructs 48 h after transfection. The construct HVR1Ala has alanine substitutions at residues 167−172. GFP-tH is an inert control protein for the assay consisting of GFP with the minimal C-terminal membrane anchor of H-ras. The results of Student's *t*-tests using mean neurite length of GFP-H-RasG12V transfected cells as the reference control are given on the graph.
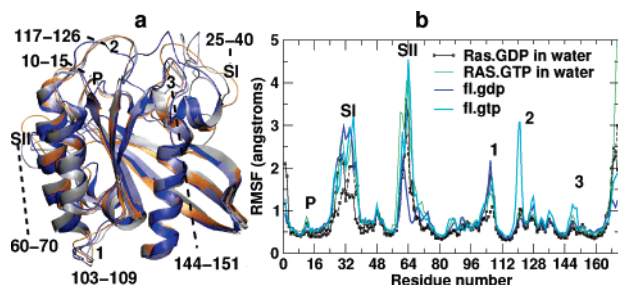
Figure 8. Dynamics of the protein soluble domain. (a) Superposition of snapshots at 0.2 ns (blue), 10 ns (light blue), 20 ns (silver), and 27 ns (orange) from simulation fl.gtp showing that significant displacements occur at loop regions. Some of these mobile segments are labeled. (b) Root-mean-squared fluctuations (RMSF) calculated for the simulations in water and in the membrane environment. Last 10 ns data are shown.

ask: do the C-terminal extension and/or the protein−membrane interactions discussed above affect the dynamics of the protein and the membrane?

Minor Effects on the G-Domain. Figure 8a shows backbone superpositions at four time points along simulation fl.gtp. We can see that, besides the switch I and switch II regions, which are known to be highly dynamic,[12] a number of loops (labeled) and the C-terminal end of α5 experienced localized structural changes. Comparison of the backbone root-mean-squared fluctuations (RMSF) calculated from the full-length simulations in membrane with those of the soluble domain in water (Figure 8b) suggests minor but potentially significant motional changes. These include reduced fluctuations at the C-terminus of α5 and enhanced dynamics at site 1 (residues 103−109). Furthermore, switch II became ordered and site 2 (residues 117−126) disordered in simulations fl.gdp and fl.gtp, respectively. Importantly, sites 2 and 3, whose structure is susceptible to change upon oncogenic mutations,[12] encompass the nucleotide binding motifs G2 and G3 that contact the guanosine base and are highly conserved among all small GTPases.

The Local Structure and Dynamics of the Membrane Is Perturbed. The order parameters in the simulations with the full-length H-Ras are slightly higher at the mid-section of the DMPC tails (Figure 2a). These small changes could be due to the constant area used in the simulations. However, the distribution of the head group at the upper leaflet is significantly wider in simulations with inserted protein (Figure 5a; the lower

leaflet is unaffected perhaps due to damping of motions by the bound protein). Furthermore, the membrane thickness is not uniform, varying in space and time (Figure 4). Mesoscopic, thermally excited undulatory and peristaltic motions of biological membranes in the liquid crystalline phase are important for many of their functions,[30] but are rarely observed in simulations because of the small length and time scales.[31] The current size (216 lipids) enabled peristaltic motions to be captured in the nanosecond time scale. Under the conditions employed, the peristaltic motion appears to be enhanced upon protein insertion. Whether the membrane responds differently in a different simulation condition (e.g., constant surface tension) is open for further investigation. Nonetheless, the observed effects of the protein on the structure and dynamics of the membrane raise a crucial question: does Ras facilitate formation of membrane microdomains essential for signaling? Along this line, a dynamic organization of Ras-induced nanoclusters has recently been proposed.[6]

Biological Implications and Concluding Remarks

The catalytic domain and the linker of H-Ras were implicated in modulating function and microdomain localization with unknown mechanism.[4,25] The simulations indicate direct protein−membrane interaction through either the catalytic domain or the linker. Such an interaction would allow transmission of structural changes from bilayer to protein and vice versa. This result is consistent with an earlier proposal, based on fluorescence resonance energy transfer studies, that the GPI-anchored ectoplacental alkaline phosphatase is located very close to, or possibly resting on, the surface of lipid bilayer.[32] Furthermore, based on crystallographic studies, a model has been forwarded for the membrane binding mechanism of a myristoylated ADP-ribosylation factor-1 (ARF-1).[33] According to this model, the myristic moiety of ARF-1 interacts with the lipid tails, while a cluster of positively charged residues interact with the phospholipid head group.[33] The fact that positively charged groups of H-Ras protein are the major source of the soluble domain−DMPC interaction is in accord with the proposed model. Our preliminary experimental results support the membrane interactions of residues R128, R135, R169, and K170.

The preceding discussions indicate that model 1 is the dominant conformation in the GDP-bound simulations and model 2 in the GTP-bound ones (the mechanism by which the nucleotides modulate the structural changes will be addressed in a forthcoming publication). However, we would like to stress that, because of insufficient sampling and the use of the activated G12V variant, the data are indicative, but not conclusive, of the conformational preferences of GDP and GTP loaded H-Ras. Results from multiple simulations suggest that membrane insertion followed by stabilization of the linker and the G-domain at the membrane surface was not always achievable in few tens of nanoseconds. This is to be expected for such a complex system. Typically, while the anchor inserts fairly quickly, the G-domain makes several attempts before finding the correct orientation for a stable binding. For example, in two of the runs, the catalytic domain did not manage to stably interact with the bilayer within 40 ns, while in others it took between 15 and 25 ns. Nevertheless, the existence of two ensembles of conformations whose corresponding average structures are represented by the two models is apparent. The relative populations of the two may be modulated by GDP/GTP exchange. Thus, with the assumption that models 1 and 2 represent GDP and GTP loaded H-Ras in physiologic conditions, as the simulations suggest, many biological properties of H-Ras
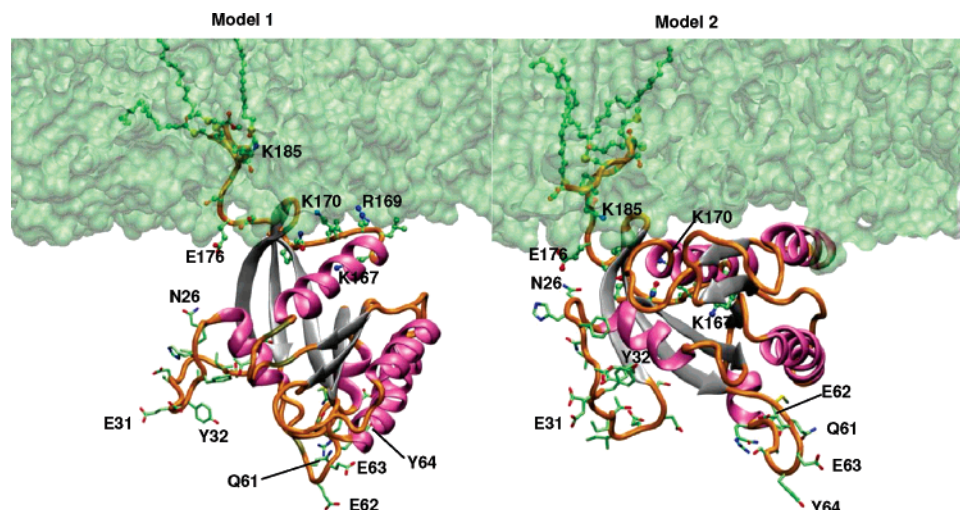
Figure 9. Models 1 and 2. Part of the membrane is represented by a transparent light green surface; the HVR residues are in ball-and-stick and the switch I and switch II residues in stick models.

can be accounted for. For example, differences in membrane subdomain compartmentalization and/or interaction with regulators and effectors were suggested to determine specificity among the H-, N-, and K-Ras proteins. Thus, to guide future studies, we provide a brief discussion of the implications of the two models in membrane microdomain compartmentalization and in binding of effector/regulator molecules.

Lateral Segregation. Membrane binding via model 1 involves deeply inserted and stretched Ras acyl chains (Figures 4 and 9), which can be more effectively accommodated by the thicker hydrophobic core of raft-like domains, and hence model 1 would have a reduced affinity to non-raft regions. In contrast, the more flexible acyl chains of model 2 could be accommodated in disordered, non-raft microdomains. This is consistent with the colocalization of GDP loaded H-Ras in raft and non-raft microdomains and the segregation of GTP loaded H-Ras to non-raft domains.[34] On the basis of biochemical and steric considerations, we can further assume that interfacial protein side chain−DMPC head group interactions facilitate segregation to non-raft microdomains. Thus, Ras in model 2 with its larger protein−membrane interfacial surface area (Figure 9) would segregate to non-raft subdomains more efficiently than does model 1. When the results on the role of the linker are combined with the deeper insertion of model 1 and the relatively interfacial localization of model 2, some of the biochemical data on the alanine mutants of the linker described previously[4] can be structurally rationalized. For instance, no specific interaction was observed between HVR2 and the bilayer, and hence its alanine substitution would not affect H-Ras−membrane interactions. Its removal, however, would bring the long R/K side chains of HVR1 too close to the bilayer surface, prohibiting effective hydrogen-bond formation with the phosphate oxygens. Moreover, side chains at the HVR1 region have preferred orientations, especially in model 1, consistent with experimental results that the specific identity of residues 167−172 is required for proper lateral segregation and effector function.[4]

Regulator and Effector Binding. The effector loop (switch I) is highly flexible and entirely solvated in both models, but its orientation relative to the membrane plane is different (Figures 6 and 9). This difference probably has a functional role related to the spatial arrangement of effector and activator molecules with respect to Ras and the membrane plane. Additionally, the two models resulted in different side-chain orientations at switches I and II. For example, Y64 at the tip of

Table 2. Simulation Systems[a]

system:	pure bilayer (DMPC)	C-term of H-Ras (res. 167−186)	full-length H-Ras[b]	
			(Mg^{2+}·GDP)	(Mg^{2+}·GTP)
sim. name	dmpc	hvr	fl.gdp	fl.gtp

[a] Only simulations involving membrane (25−40 ns) are shown, whereas simulations performed for only the soluble domain of the protein in water (10−15 ns long) are not. Coordinates of the GDP-bound G12V variant of H-Ras (entry 2Q21[26]) were downloaded from the protein data bank.[41] [b] Although simulations were run in triplicates differing only in the assignment of initial velocities, the discussions presented here focus on the best equilibrated runs.

switch II, which is one of the critical residues involved in GAP[15] and effector phosphoinositide 3-kinase γ[35] binding, sticks out to solvent in model 2 but not in model 1 (Figure 9). Furthermore, the accessibility of the linker in the two models is entirely different. The linker modulates interaction with effector, GEF and possibly GAP,[4,25] as well as ubiquitination[36] of plasma membrane-bound H-Ras. Thus, the models presented here open exciting new opportunities for future investigations of Ras binding to its regulators and effectors.

In summary, in this paper we have characterized the interactions of H-Ras with a membrane and presented two models for the complex structure. The roles of the catalytic domain and the linker in membrane binding, as well as the details of the interactions that govern membrane binding, have been discussed. The results support the available experimental data on Ras and related systems and provide the basis for future experimental and computational investigation of membrane localization and signaling specificity. Most importantly, the results pave the way for a structure-based design of selective anti-cancer agents. The proposals presented here are strongly supported by the initial experiments so far carried out. Further experiments are in progress.

Methods

The full-length H-Ras in a DMPC bilayer was simulated in the Mg^{2+}·GDP (fl.gdp) and Mg^{2+}·GTP (fl.gtp) complexed forms (Table 2). To study the effect of the soluble domain on membrane insertion, an additional simulation (hvr) of only the hypervariable segment (residues 167−186, HVR) was carried out. For comparison of the membrane structure in the presence and absence of the protein, a free DMPC bilayer was simulated under identical conditions (dmpc). All system setups and equilibrations were performed with the CHARMM program,[37] and production simulations were performed with NAMD.[38]

Force Field. The CHARMM27 force field[39] was used in all simulations. As described before,[20] parameters for the lipidated "residues" were built by analogy (e.g., with those of palmitic acid and Cys). Similarly, parameters of ADP/ATP were used as a reference for the GDP/GTP nucleotides.

Modeling and Simulation Setup. Full-Length H-Ras Protein. The model membrane used in this study, a DMPC bilayer at the liquid crystalline phase (310 K), represents the "disordered" region of a plasma membrane. However, the GDP bound wild-type H-Ras preferentially localizes at cholesterol-dependent "ordered" surface domains or lipid-rafts.[34,40] Therefore, we used the G12V variant that segregates to non-raft microdomains.[40] Thus, an X-ray structure of Mg^{2+}·GDP-bound G12V H-Ras (H-RasG12V) comprising residues 1–171 (code 2Q21[26]) was downloaded from the protein data bank.[41]

The missing residues (172–186) were modeled as follows. First, a C-terminally oxymethylated linear structure made up of all of the missing amino acids was manually built. The palmitoyl thioester (at Cys181 and Cys184) and hexadecyl thioether (at Cys186) were attached. Note that the saturated hexadecyl group models the unsaturated farnesyl with minimal effect on the function and membrane-binding properties of Ras.[19,42] The extended structure was subjected to a series of CHARMM[37] energy minimizations: (i) 500 steps of steepest decent (SD) with all except the lipid-modified "residues" held fixed, (ii) 600 steps of SD and 600 steps of conjugate gradient (conj) minimizations with the regular (non-lipidated) amino acids harmonically constrained (force constant of 10 kcal/mol/Å), and (iii) 600 steps of SD and 600 steps of conj with all residues free. The resulting conformation was ligated onto the X-ray structure. Bad atomic contacts were again relieved by three cycles of 500 SD followed by 500 steps of conj with all except residues 167–186 held fixed, harmonically constrained, and set free, respectively. The resulting structure is shown in Figure 1a. The Mg^{2+}·GTP-bound H-Ras starting structure was obtained by addition and local optimization of the γ-phosphate onto the Mg^{2+}·GDP of the same 1Q21 X-ray structure. Thus, any difference between the two simulations should originate solely from the GDP/GTP exchange.

DMPC Bilayer. Based on the last snapshot of an earlier 6 ns simulation of free DMPC,[20] a bilayer of 108 lipids per leaflet (87.2 and 74.1 Å along the x and y directions, i.e., an area per lipid of 59.8 Å^2 (refs 43, 44)) was constructed. The rectangular shape and lateral dimension of the bilayer was chosen to accommodate the full-length H-Ras protein in the multicomponent simulations (see below). Each leaflet was solvated by a slab of 4590 TIP3 water molecules.

H-Ras−DMPC Complex. The same lateral dimensions and number of lipids as in the free DMPC bilayer were used. However, because the protein is to be inserted into the lower leaflet, the water slab at this leaflet was enlarged along the z-axis so that protein atoms will be at least 10 Å away from the sides of the slab. Although spontaneous insertion is not possible in the time scales accessible by MD, we have shown earlier that membrane insertion and stabilization of a lipidated heptapeptide is ensured if 5−7 initial carbon−carbon contacts are formed between the DMPC and the Ras lipids.[20] Therefore, the protein is placed at the center and was translated and rotated until at least seven acyl carbons of a Ras lipid tail are inserted into the hydrophobic core of the DMPC lipids. To avoid strain of the bilayer due to the insertion of the "foreign" lipids, a single DMPC lipid that is closest to the Ras lipids was removed. Counter ions were added to achieve electroneutrality. The total number of atoms was 57 810 and ∼75 300 for the HVR−DMPC and full-length Ras−DMPC systems, respectively (see Figure 1b).

Molecular Dynamics. Each of the systems prepared as described above was relaxed by three cycles of 50 steps Advanced Basis Newton Raphson (ABNR) minimizations applying harmonic constraints of force constants 50 (20), 5 (2), and 5 (0) kcal mol^{-1}/Å to the solute (water) heavy atoms. Note that solute includes the protein and lipid atoms. Equilibration at 310 K for 40 ps with uniform rescaling of atomic velocities and for a further 200 ps with Gaussian distribution of velocities was done in the NVT ensemble (i.e., constant number of particles (N), volume (V), and temperature (T)). We used an NPTA ensemble for the production phase: constant T (maintained by Nose−Hoover temperature control[45]), normal pressure (P, Berendsen control), and cross-sectional area (A).[46] Periodic boundary conditions with full particle-mesh Ewald electrostatics,[47] a 12 Å cutoff for the vdW interactions, and 14 Å for nonbonded list update, were used in all simulations. Use of the SHAKE algorithm to constrain bonds involving hydrogens enabled an integration time step of 2 fs to be used.

Analysis. The programs CHARMM,[37] VMD,[48] and WORDOM (M. Seeber, personal communications) were used for most of the analysis. The molecular order parameter, S_{CD}, was calculated as:

$$S_{CD} = \frac{1}{2}\langle 3 \cos^2 \theta_n - 1 \rangle \tag{1}$$

where θ_n is the instantaneous angle between a vector along the methylene/methyl hydrogens of the acyl chains and the bilayer normal (i.e., the angle between the CH vector and the bilayer normal).

The average bilayer thickness ($D_{PP}(z)$) is defined as the separation along the membrane normal between the average location of the phosphorus atoms at each monolayer:

$$D_{PP}(z) = \langle P(z;\text{leaf1}) - P(z;\text{leaf2}) \rangle \tag{2}$$

where $P(z;\text{leaf1})$ and $P(z;\text{leaf2})$ represent the average phosphorus atom location at leaflet 1 (top, positive) and leaflet 2 (bottom, negative) relative to the bilayer center at $z = 0.0$.

Similarly, the hydrophobic thickness ($L_{C2:C2}(z)$) is defined as the average separation between the second carbon atoms across the two leaflets,

$$L_{C2:C2}(z) = \langle C2(z;\text{leaf1}) - C2(z;\text{leaf2}) \rangle \tag{3}$$

The chain length ($L_{C2:C14}(z)$) is the average separation between the second and the last carbon atoms of the lipids averaged over the entire system

$$L_{C2:C14}(z) = \langle C2(z) - C14(z) \rangle \tag{4}$$

Note that $L_{C2:C14}(z)$ defined here does not include the correction value of 1.53 Å to account for the distance from the first methylene to the carbonyl carbon (0.55 Å) and the extra length of the terminal methyl group (0.98 Å).[49]

PC12 Differentiation Assays. Mutation of H-Ras residues R128, R135, R169, and K170 was performed by site directed mutagenesis of GFP-H-RasG12V[25] or mCFP-H-RasG12V. All constructs were verified by DNA sequencing. PC12 cells were cultured in DMEM supplemented with 25 mM Hepes, pH 7, 10% horse serum, 5% donor calf serum, and 2 mM glutamine at 37 °C and 5% CO$_2$. On day one, cells were seeded onto poly-L-lysine (Sigma)-coated coverslips at about 25% confluence. The following day, cells were transiently lipofected in Optimem according to the manufacturer's instructions (Invitrogen). Cells were returned to maintenance medium 16 h after transfection and then incubated for another 48 h before fixation in 4% paraformaldehyde at room temperature for 30 min. 100 cells on each of two coverslips were counted as either differentiated or undifferentiated as described previously;[25] in addition, 26 cells on each of two coverslips were imaged to determine the mean neurite length per cell. Neurite length was measured in Image J, and differences between H-RasG12V and mutant H-RasG12V transfected cells were evaluated for statistical significance using Student's t-test.

References

(1) Herrmann, C. Ras-effector interactions: after one decade. *Curr. Opin. Struct. Biol.* **2003**, *13*, 122−129.

(2) Spoerner, M.; Herrmann, C.; Vetter, I. R.; Kalbitzer, H. R.; Wittinghofer, A. Dynamic properties of the Ras switch I region and its importance for binding to effectors. *Proc. Natl. Acad. Sci. U.S.A.* **2001**, *98*, 4944−4949.

(3) Hancock, J. F.; Magee, A. I.; Childs, J. E.; Marshall, C. J. All ras proteins are polyisoprenylated but only some are palmitoylated. *Cell* **1989**, *57*, 1167−1177.

(4) Rotblat, B.; Prior, I. A.; Muncke, C.; Parton, R. G.; Kloog, Y.; Henis, Y. I.; Hancock, J. F. Three separable domains regulate GTP-dependent association of H-Ras with the plasma membrane. *Mol. Cell. Biol.* **2004**, *24*, 6799−6810.

(5) Hancock, J. F.; Parton, R. G. Ras plasma membrane signalling platforms. *Biochem. J.* **2005**, *389*, 1−11.

(6) Plowman, S. J.; Muncke, C.; Parton, R. G.; Hancock, J. F. H-Ras, K-Ras, and inner plasma membrane raft proteins operate in nano-clusters with differential dependence on the actin cytoskeleton. *Proc. Natl. Acad. Sci. U.S.A.* **2005**, *102*, 15500−15505.

(7) Brunger, A. T.; Milburn, M. V.; Tong, L.; de Vos, A. M.; Jancarik, J.; Yamaizumi, Z.; Nishimura, S.; Ohtsuka, E.; Kim, S. H. Crystal structure of an active form of Ras protein, a complex of a GTP analog and the Hras p21 catalytic domain. *Proc. Natl. Acad. Sci. U.S.A.* **1990**, *87*, 4849−4853.

(8) Pai, E. F.; Kabsch, W.; Krengel, U.; Holmes, K. C.; John, J.; Wittinghofer, A. Structure of the guanine-nucleotide-binding domain of the Ha-Ras oncogene product p21 in the triphosphate conformation. *Nature* **1989**, *341*, 209−214.

(9) Milburn, M. V.; Tong, L.; de Vos, A. M.; Brunger, A.; Yamaizumi, Z.; Nishimura, S.; Kim, S. H. Molecular switch for signal transduction: structural differences between active and inactive forms of protooncogenic Ras proteins. *Science* **1990**, *247*, 939−945.

(10) Spoerner, M.; Nuehs, A.; Ganser, P.; Herrmann, C.; Wittinghofer, A.; Kalbitzer, H. R. Conformational states of Ras complexed with the GTP analogue GppNHp or GppCH2p: implications for the interaction with effector proteins. *Biochemistry* **2005**, *44*, 2225−2236.

(11) Kraulis, P. J.; Domaille, P. J.; Campbell-Burk, S. L.; Akenn, T. V.; Laue, E. D. Solution structure and dynamics of Ras p21.GDP determined by heteronuclear three- and four-dimensional NMR spectroscopy. *Biochemistry* **1994**, *33*, 3515−3531.

(12) Krengel, U.; Schlichting, L.; Scherer, A.; Schumann, R.; Frech, M.; John, J.; Kabsch, W.; Pai, E. F.; Wittinghofer, A. Three-dimensional structures of H-Ras p21 mutants: molecular basis for their inability to function as signal switch molecules. *Cell* **1990**, *62*, 539−548.

(13) Iuga, A.; Spoerner, M.; Kalbitzer, H. R.; Brunner, E. Solid-state 31P NMR spectroscopy of microcrystals of the Ras protein and its effector loop mutants: comparison between crystalline and solution state. *J. Mol. Biol.* **2004**, *342*, 1033−1040.

(14) Spoerner, M.; Wittinghofer, A.; Kalbitzer, H. R. Perturbation of the conformational equilibria in Ras by selective mutations as studied by 31P NMR spectroscopy. *FEBS Lett.* **2004**, *578*, 305−310.

(15) Scheffzek, K.; Ahmadian, M. R.; Kabsch, W.; Wiesmuller, L.; Lautwein, A.; Schmitz, F.; Wittinghofer, A. The Ras-RasGAP complex: structural basis for GTPase activation and its loss in oncogenic Ras mutants. *Science* **1997**, *277*, 333−338.

(16) Boriack-Sjodin, P. A.; Margarit, S. M.; Bar-Sagi, D.; Kuriyan, J. The structural basis of the activation of Ras by Sos. *Nature* **1998**, *394*, 337−343.

(17) Hall, B. E.; Yang, S. S.; Boriack-Sjodin, P. A.; Kuriyan, J.; Bar-Sagi, D. Structure-based mutagenesis reveals distinct functions for Ras switch 1 and switch 2 in SOS-catalyzed guanine nucleotide exchange. *J. Biol. Chem.* **2001**, *276*, 27629−27637.

(18) Thapar, R.; Williams, J. G.; Campbell, S. L. NMR characterization of full-length farnesylated and non-farnesylated H-Ras and its implications for Raf activation. *J. Mol. Biol.* **2004**, *343*, 1391−1408.

(19) Huster, D.; Vogel, A.; Katzeka, C.; Sheidt, H. A.; Binder, H.; Dante, S.; Gutberlet, T.; Schoernig, O.; Waldmann, H.; Arnold, K. Membrane insertion of a lipidated Ras peptide studied by FTIR, solid-state NMR, and neutron diffraction spectroscopy *J. Am. Chem. Soc.* **2003**, *125*, 4070−4079.

(20) Gorfe, A. A.; Pellarin, R.; Caflisch, A. Membrane localization and flexibility of a lipidated Ras peptide studied by molecular dynamics simulations. *J. Am. Chem. Soc.* **2004**, *126*, 15277−15286.

(21) Vogel, A.; Katzka, C. P.; Waldmann, H.; Arnold, K.; Brown, M. F.; Huster, D. Lipid modifications of a Ras peptide exhibit altered packing and mobility versus host membrane as determined by ^{2}H solid-state NMR *J. Am. Chem. Soc.* **2005**, *127*, 12263−12272.

(22) Allen, T. W.; Andersen, O. S.; Roux, B. Energetics of ion conduction through the gramicidin channel. *Proc. Natl. Acad. Sci. U.S.A.* **2004**, *101*, 117−122.

(23) Böckmann, R. A.; Caflisch, A. Spontaneous formation of detergent micelles around the outer membrane protein OmpX. *Biophys. J.* **2005**, *8*, 3191−3204.

(24) Rocks, O.; Peyker, A.; Kahms, M.; Verveer, P. J.; Koerner, C.; Lumbierres, M.; Kuhlmann, H.; Waldmann, H.; Wittinghofer, A.; Bastiaens, P. I. An acylation cycle regulates localization and activity of palmitoylated Ras isoforms. *Science* **2005**, *307*, 1746−1752.

(25) Jaumot, M.; Yan, J.; Clyde-Smith, J.; Sluimer, J.; Hancock, J. F. The linker domain of the H-Ras hypervariable region regulates interactions with exchange factors, Raf-1 and phosphoinositide 3-kinase. *J. Biol. Chem.* **2002**, *277*, 272−278.

(26) Tong, L. A.; de Vos, A. M.; Milburn, M. V.; Kim, S. H. Crystal structures at 2.2 Å resolution of the catalytic domains of normal Ras protein and an oncogenic mutant complexed with GDP. *J. Mol. Biol.* **1991**, *217*, 503−516.

(27) Brandt-Rauf, P. W.; Carty, R. P.; Chen, J. M.; Lee, G.; Rackovsky, S.; Pincus, M. R. The structure of the carboxyl terminus of the p21 protein. Structural relationship to the nucleotide-binding/transforming regions of the protein. *J. Protein Chem.* **1990**, *9*, 137−142.

(28) Baker, T. L.; Zheng, H.; Walker, J.; Coloff, J. L.; Buss, J. E. Distinct rates of palmitate turnover on membrane-bound cellular and onco-genic H-ras. *J. Biol. Chem.* **2003**, *278*, 19292−19300.

(29) Roy, S.; Plowman, S.; Rotblat, B.; Prior, I.; Muncke, C.; Grainger, S.; Parton, R. G.; Henis, Y. I.; Kloog, Y.; Hancock, J. F. Individual palmitoyl residues serve distinct roles in H-Ras trafficking, microlo-calization, and signaling. *Mol. Cell. Biol.* **2005**, *25*, 6722−6733.

(30) Safran, S. A. *Statistical Thermodynamics of Surfaces, Interfaces, and Membranes*; Addison-Wesley, New York: Reading, MA, 1994.

(31) Lindahl, E.; Edholm, O. Mesoscopic undulations and thickness fluctuations in lipid bilayers from molecular dynamics simulations. *Biophys. J.* **2000**, *79*, 426−433.

(32) Lehto, M. T.; Sharom, F. J. Proximity of the protein moiety of a GPI-anchored protein to the membrane surface: a FRET study. *Biochemistry* **2002**, *41*, 8368−8376.

(33) Greasley, S. E.; Jhoti, H.; Teahan, C.; Solari, R.; Fensome, A.; Thomas, G. M.; Cockcroft, S.; Bax, B. The structure of rat ADP-ribosylation factor-1 (ARF-1) complexed to GDP determined from two different crystal forms. *Nat. Struct. Biol.* **1995**, *2*, 797−806.

(34) Plowman, S. J.; Hancock, J. F. Ras signaling from plasma membrane and endomembrane microdomains. *Biochim. Biophys. Acta* **2005**, *1746*, 274−283.

(35) Pacold, M. E.; Suire, S.; Perisic, O.; Lara-Gonzalez, S.; Davis, C. T.; Walker, E. H.; Hawkins, P. T.; Stephens, L.; Eccleston, J. F.; Williams, R. L. Crystal structure and functional analysis of Ras binding to its effector phosphoinositide 3-kinase γ. *Cell* **2000**, *103*, 931−943.

(36) Jura, N.; Scotto-Lavino, E.; Sobczyk, A.; Bar-Sagi, D. Differential modification of Ras proteins by ubiquitination. *Mol. Cell* **2006**, *21*, 679−87.

(37) Brooks, B. R.; Bruccoleri, R. E.; Olafson, B. D.; States, D. T.; Swaminathan, S.; Karplus, M. CHARMM − A program for mac-romolecular energy, minimization, and dynamics calculations *J. Comput. Chem.* **1983**, *4*, 187−217.

(38) Phillips, J. C.; Braun, R.; Wang, W.; Gumbart, J.; Tajkhorshid, E.; Villa, E.; Chipot, C.; Skeel, R. D.; Kale, L.; Schulten, K. Scalable molecular dynamics with NAMD. *J. Comput. Chem.* **2005**, *26*, 1781−1802.

(39) MacKerell, A. D.; et al. All-atom empirical potential for molecular modeling and dynamics studies of proteins. *J. Phys. Chem. B* **1998**, *102*, 3586−3616.

(40) Parton, R. G.; Hancock, J. F. Lipid rafts and plasma membrane microorganization: insights from Ras. *Trends Cell Biol.* **2004**, *14*, 141−147.

(41) Berman, H. M.; Westbrook, J.; Feng, Z.; Gilliland, G.; Bhat, T. N.; Weissig, H.; Shindyalov, I. N.; Bourne, P. E. The protein data bank. *Nucleic Acids Res.* **2000**, *28*, 235−242.

(42) Hinterding, K.; Alonso-Diaz, D.; Waldmann, H. Organic synthesis and biological signal transduction. *Angew. Chem., Int. Ed.* **1998**, *37*, 688−749.

(43) Petrache, H. I.; Dodd, S. W.; Brown, M. F. Area per lipid and acyl length distributions in fluid phosphatidylcholines determined by (2)H NMR spectroscopy. *Biophys. J.* **2000**, *79*, 3172−3192.

(44) Kucerka, N.; Kiselev, M. A.; Balgavy, P. Determination of bilayer thickness and lipid surface area in unilamellar dimyristoylphosphatidylcholine vesicles from small-angle neutron scattering curves: a comparison of evaluation methods. *Eur. Biophys. J.* **2003**, *33*, 328−334.

(45) Hoover, W. G. Canonical dynamics: Equilibrium phase-space distributions. *Phys. Rev. A* **1985**, *31*, 1695−1697.

(46) Feller, S. E.; Pastor, R. W. Constant surface tension simulations of lipid bilayers: The sensitivity of surface areas and compressibilities. *J. Phys. Chem.* **1999**, *111*, 1281−1287.

(47) Essmann, U.; Perera, L.; Berkowitz, M. L.; Darden, T.; Lee, H.; Pedersen, L. G. A smooth particle mesh ewald method. *J. Chem. Phys.* **1995**, *151*, 8577−8593.

(48) Humphrey, W.; Dalke, A.; Schulten, K. VMD - Visual molecular dynamics. *J. Mol. Graphics* **1996**, *14*, 33−38.

(49) Petrache, H. I.; Tu, K.; Nagle, J. F. Analysis of simulated NMR order parameters for lipid bilayer structure determination. *Biophys. J.* **1999**, *76*, 2479−2487.

(50) Tristram-Nagle, S.; Nagle, J. F. Lipid bilayers: thermodynamics, structure, fluctuations, and interactions. *Chem. Phys. Lipids* **2004**, *127*, 3−14.

(51) Kucerka, N.; Liu, Y.; Chu, N.; Petrache, H. I.; Tristram-Nagle, S.; Nagle, J. F. Structure of fully hydrated fluid phase DMPC and DLPC lipid bilayers using X-ray scattering from oriented multilamellar arrays and from unilamellar vesicles. *Biophys. J.* **2005**, *88*, 2626−2637.